technische universität
dortmund

Revision of the multiple scattering algorithms in PROPOSAL

Bachelorarbeit
zur Erlangung des akademischen Grades
Bachelor of Science

vorgelegt von
Malte Geisel-Brinck
geboren in Witten

Lehrstuhl für Experimentelle Physik V
Fakultät Physik
Technische Universität Dortmund
2013

1. Gutachter : Prof. Dr. Dr. Wolfgang Rhode

2. Gutachter : Prof. Dr. Bernhard Spaan

Datum des Einreichens der Arbeit: 05. November 2013

Abstract

This bachelor thesis is summarizing the work that has been done on PROPOSAL by the author. PROPOSAL is a particle transport simulation program designed for the use in the Monte Carlo chain of the IceCube experiment, but as well applicable to different contexts.
In order to take account of recent and future low-energy upgrades to IceCube (DeepCore and PINGU), the effect of multiple scattering has been reviewed. Thereby, it was found that the current implementation in PROPOSAL was incorrect. Hence Molière's theory of multiple scattering and its Highland approximation are summarized and practical and easy computation methods are presented.
Finally, both parametrizations are checked against each other and compared with measurement data.

Contents

1 Introduction

This thesis is outlining the work on the software tool PROPOSAL done by the author. As a result, the multiple scattering algorithms have experienced a total makeover.

In order to point out the context of the thesis, an overview of the IceCube experiment and its physical relevance is given in this chapter. Eventually, PROPOSAL and the use of multiple scattering theories is described. In the following chap. 2 , Molière's theory of multiple scattering and Highland's approximation are summarized in detailed and up-to-date fashion. This is to author modern and practical reference material for further work on PROPOSAL. An easy and fast method to calculate Molière's distribution and draw random numbers out of it was developed. Since a revision revealed that the implemented multiple scattering algorithm used in MMC and PROPOSAL was incorrect, a new and easier one based on Highland's formula was implemented, too. That is altogether described in chap. 3 . Finally, both parametrizations are checked and compared in chap. 4 .

1.1 Astroparticle physics

Human kind's studies of the universe are based on the information it is providing. In astronomy, the traditional way to explore the surrounding cosmos always was to draw information from the spectrum of visible light reaching earth.

Starting from the discovery of cosmic rays by Hess in the early 1910s, the set of information carriers to be analysed has been enhanced by several (partly new discovered) particles over the last hundred years. Modern experimental astroparticle physics mostly focusses on charged cosmic rays like protons, electrons and ions (e.g. the Pierre Auger Observatory [1]), high-energy γ-rays (e.g. the MAGIC telescope [2]) and neutrinos like the IceCube experiment [3]. Especially in the latter project, not only the origin, spectra and propagation through space, but as well particle physical issues are of importance [4].

1.2 Neutrino astronomy

Among the information carrying particles observed by telescopes in astroparticle physics, neutrinos are yet the most unknown. Still, they are expected to have big potential to contribute decisively to the answering of central questions in modern astrophysics.

High-energy neutrinos originate from high-energy collisions of charged cosmic rays with hadrons (matter) [5]. Only interacting through the weak interaction, their extraordinary small cross sections in terms of interactions with matter allow them to escape optical dense objects [6] (e.g. dust clouds). In contrast to charged cosmic rays, they are not affected by magnetic or electric fields in between. Thus energy and direction information about the origin are still preserved when they are detected on earth.

On the other hand, the low interaction probability makes the detection of neutrinos technically extremely difficult and leads to the need of detectors of at least cubic kilometer dimensions [5]. This is applied in telescopes such as ANTARES [7], IceCube (see below) and the future project KM3NeT (**Cubic K**ilo**M**etre **Ne**utrino **T**elescope [8]).

1.3 IceCube

The IceCube experiment is located in the Antarctica and currently the world's largest neutrino detector. As a follow-on project to the AMANDA experiment (**A**ntarctic **M**uon **A**nd **N**eutrino **D**etector **A**rray [9], operative until 2006), its build-up was completed in December 2010 [3].

IceCube's underlying concept is to observe high-energy neutrinos indirectly by detecting charged secondary particles produced in neutrino interactions. This is possible, since they and some of the secondary particles they produce in the medium emit Cherenkow light when traversing matter at a velocity that is greater than the speed of light inside the medium. Especially interactions producing muons are of interest, since these leave the longest and best reconstructable tracks inside the detector [10].

Due to the rareness of neutrino interactions with matter, a large volume of an optical transparent medium is needed to apply this method. Therefore, IceCube is located between 1450 m and 2450 m depth in the highly transparent ice of the geographic South Pole. In its current state, it is containing 86 so called strings, each attached with 60 DOMs (**D**igital **O**ptical **M**odules contain photomultiplier tubes), that are spread over a volume of about 1 km^3 [3].

A surface air shower array is used to study cosmic rays and identify atmoshperical muons (IceTop [11]). Additionally, the detector consists of the DeepCore extension. It was installed in order to lower IceCube's sensitivity to neutrino energies down to 10 GeV [12]. Another extension named PINGU (**P**recision **I**ceCube **N**ext **G**eneration **U**pgrade) is yet under consideration to lower this threshold even further [13].

IceCube is designed for the study of candidates for being sources of the cosmic-ray spectrum. Objects considered as such are, for example, supernova remnants (SNRs), gamma-ray bursts (GRBs) and regions in the vicinity of black holes. Further scientific goals are the search for dark matter [3] and the examination of neutrino properties (e.g. neutrino oscillation and mass hierarchy with PINGU [13]).

1.4 PROPOSAL

In order to reconstruct particle tracks properly and make sense of data produced by the photomultiplier tubes in IceCube and similar detectors (see above), extensive computer simulations are required. The typical Monte Carlo simulation chain used for this purpose can be structured into three parts: 1. The *generator* creates cosmic particles

and propagates them to the detector, along with their secondary particles produced in interactions with the atmosphere. 2. From there on, the *propagator* simulates the passage of the generated particles through the detector medium. 3. Finally, the response of the *detector* interacting with the generated Cherenkow photons is computed.

Since background signals are expected to be 3-5 orders of magnitude larger than the sought neutrino signals, a large amount of simulation data that should be as accurate as possible is needed for separating signals from the noise properly [6].

For this purpose, the Java-based program **M**uon **M**onte **C**arlo (MMC) is currently used by the IceCube collaboration to propagate charged leptons through the Antarctic ice of the detector [14]. It is about to be replaced by its successor, the **PR**opagator with **O**ptimal **P**recision and **O**ptimized **S**peed for **A**ll **L**eptons, also called PROPOSAL. Therefore, the implementations of MMC have been translated into an object orientated C++-structure, revised and optimized in terms of computation speed. Hence, it allows a better integration into the C++-based simulation chains of projects such as IceCube and ANTARES [6].

Due to recently installed and upcoming low-enery extensions to IceCube (e.g. PINGU) and other possible fields of application for PROPOSAL, the validity of implemented algorithms is to be revised for smaller particle energies ($\sim$ 1 GeV). This thesis is focussing on the effect of multiple scattering that is inversely correlating with the particle momentum p as it is pointed out in the following chapters.

1.5 Multiple scattering

In particle physics, the term "scattering" is defined as "a change in the direction of motion of a particle because of a collision with another particle" [15]. For the regarded case here, that means the interactions of a charged lepton with the particles of an (in good approximation) stationary atom of the target material.

There is talk of multiple scattering when a large number of single (maybe simultanious) scatterings is adding up. That applies to passages of particles through sufficiently thick layers of matter [16].

Several theories have been developed to describe the outcome of multiple scattering of charged leptons by angular probability distributions (e.g. [17–19]). Among these, the theory of Gerd Molière (1947) results from a derivation that stays analytical until the end [16, 20]. Although the whole physics of the elastic scatter is covered by the determination of only two parameters (χ_c and B), it is providing relatively good agreement with measurement data (see chap. 4). Therefore, it is still favored in most modern transport codes [21].

At this point it has to be remarked that the parametrization that was referred to as "Molière scattering" in MMC [14] and subsequently PROPOSAL [6], was actually employing Highland's formula, a semianalytical gaussian approximation to Molière's distribution [22].

In the transport code of PROPOSAL, multiple scattering is employed to calculate the displacement of a particle from its incident direction after traversing a particular thickness of a medium.
While propagating particles through a medium, the main interactions - ionization, bremsstrahlung, photonuclear interaction and pair production - are taking into account. Since the energies of most interactions are very low, such that effectively only their sum is important, interactions below a certain absolute (e_{cut}) or relative (v_{cut}) energy threshold (except bremsstrahlung) are treated continously. This procedure is crucially reducing the necessary computing time. Interactions above the threshold appear stochastically. Hence, the particle's displacement is calculated by assuming elastical multiple scatterings each time over the distance between two stochastically treated interactions [6].

Given the dominant role in the IceCube experiment, this thesis concentrates on muons as scattered particles. The implemented algorithms are as well applicable to electrons [23]. An adaptability to taus is assumed, since experiments on protons and even heavier ions showed good agreement with Molière's theory [24, 25].

Remark: All modifications described here are to be applied to the version of PROPOSAL that is referred to by [6].

2 Molière's theory

In this chapter, Molière's theory of multiple scattering based on his single scattering law is summarized. Because of several copying mistakes and misprints in papers quoting from Molière's original work [16, 20] and different systems of units (Molière published in CGS-Gauß units) the occurring formulae have been double-checked and converted into the SI system of units if needed. Since notations, nomenclatures and definitions of functions used in older publications were occasionally outdated, listed formulae may look different from the orignal ones in [16, 20], but are resulting in same values.

2.1 Single scattering

Molière bases his theory of multiple scattering on his own theory of the single scattering of fast charged particles in a screened Coulomb field. This adaptation of single scattering is described in [20].

Since the occurring scattering angles are expected to be sufficiently small ($\chi < 20°$) the approximation $\chi \approx \sin\chi$ is quite accurate.

Molière also states that in the limit of small angles the influence of spins is negligible. Thus his theory is based on the relativistic Klein-Gordon equation

$$(\Delta + k(r)^2) \cdot \psi = 0 \, . \tag{2.1.1}$$

Here, the generalized wavenumber $k(r)$ can be approximated by a second order expansion ($\sqrt{1-x} = 1 - \frac{x}{2} - \frac{x^2}{8} - \cdots$) and the neglection of the summand $\frac{-V(r)^2}{2E}$:

$$k(r) = \frac{1}{\hbar c}\sqrt{[E - V(r)]^2 - m^2c^4} \tag{2.1.2}$$

$$\approx k_0 \left[1 - \frac{V(r)}{\hbar k_0 v} - \frac{1}{2}\left(\frac{V(r)}{\hbar k_0 v}\right)^2 - \cdots\right] \tag{2.1.3}$$

where $k_0 = \frac{p}{\hbar}$ is the particle's wavenumber in a vacuum and v its speed.

A ray optical approximation (WKB method) is employed to describe the actual scatter in the vicinity of the scattering atom. The approximation becomes more and more accurate for reducing wavelengths λ . Hence, close to the atom (located at the origin) the trajectory of a scattered particle is described by straight lines and propagated as a wave from a distance z_0 on (see Fig. 1). Here, the potential is effectively $V(r \geq z_0) = 0$. Thus an incident plane wave $e^{ik_0 z}$ propagating in z-direction receives a phase shift $\phi(\rho)$ by the elastic scattering on $V(r)$. Depending on the impact parameter ρ it can be calculated as

$$\phi(\rho) = \int_{-\infty}^{\infty} \left[k(r = \sqrt{z^2 + \rho^2}) - k_0\right] dz \tag{2.1.4}$$

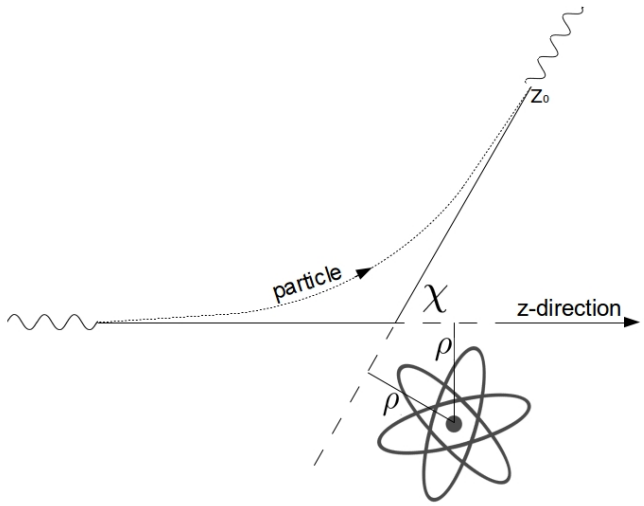

Figure 1: Ray optical approach: the trajectory of an incident particle is approximated by straight lines; ρ impact parameter; χ scattering angle

with $k(r)$ as in (2.1.3) .

In the plane $r = z_0$, the outgoing wave function is known to be

$$\psi(z_0, \rho) \;=\; \exp\left(i[k_0 z_0 + \phi(\rho)]\right) \tag{2.1.5}$$

($z_0 \sim$ atomic radius a, the exact value is not important). From there on ψ is to be propagated according to the homogeneous wave equation

$$\Delta\psi + k_0^2\psi \;=\; 0 \tag{2.1.6}$$

and evaluated at a far distant point $\vec{R}$ whose connection by a straight line ($|R| \gg z_0$) to the center of scattering has a small angle χ with the z-axis. Using Green's second identity employing the help function

$$\varphi(\vec{r}) \;=\; \frac{1}{|\vec{R} - \vec{r}|} \mathrm{e}^{ik_0|\vec{R}-\vec{r}|} \tag{2.1.7}$$

and after the substraction of the incidental wave's part, the scattered wave calculates at $\vec{R}$ as the surface integral

$$\psi_{\mathrm{scat}}(\vec{R}) \;=\; \frac{\mathrm{e}^{ik_0 z_0}}{4\pi} \oint\limits_{S(z_0)} \left[\frac{\partial\varphi}{\partial\vec{n}} + ik_0\varphi\right] \left[\mathrm{e}^{i\phi(\rho)} - 1\right] \mathrm{d}S \;. \tag{2.1.8}$$

By reducing the surface to the dominating part (∼atomic size) cylindrical coordinates (z_0, ρ and γ the azimuth angle) can be used for its approximate parametrization. Exploiting the smallness of χ and neglecting terms of the order $\frac{1}{R^2}$ the directional derivative in (2.1.8) becomes $\frac{\partial\varphi}{\partial\vec{n}} \approx ik_0\varphi$. Using $|\vec{R}-\vec{r}| \approx R - z_0 - \rho\chi\cos\gamma$ and $|\vec{R}-\vec{r}|^{-1} \approx R^{-1}$ Eqn. (2.1.8) simplifies to

$$\psi_{\text{scat}}(\vec{R}) \;=\; ik_0 \frac{\mathrm{e}^{ik_0 R}}{R} \int_0^\infty \mathrm{d}\rho\ \rho \left[\mathrm{e}^{i\phi(\rho)} - 1\right] \int_0^{2\pi} \mathrm{d}\gamma\ \frac{1}{2\pi} \mathrm{e}^{-ik_0\rho\chi\cos\gamma}\ . \tag{2.1.9}$$

The integration over γ gives the Bessel function $J_0(k_0\rho\chi)$.

From (2.1.9) the scattering cross section for the angle χ is derived by

$$Q(\chi) \;=\; R^2\,|\psi_{scat}(\chi)|^2 \tag{2.1.10}$$

$$\;=\; k_0^2 \left| \int_0^\infty \mathrm{d}\rho\ \rho J_0(k_0\rho\chi) \left[\mathrm{e}^{i\phi(\rho)} - 1\right] \right|^2 \tag{2.1.11}$$

where the potential $V(r)$ enters the equation by the phase shift $\phi(\rho)$.

Here, Molière chooses the Thomas-Fermi parametrization that is basically the Coulomb potential of a charge $\pm ze$ in a field of a positive point charge Ze (=nuleus) multiplied by a correction factor describing the electronic screening $\omega(r/a)$, the Thomas-Fermi function:

$$V(r) \;=\; \frac{1}{4\pi\epsilon_0} \frac{\pm zZe^2}{r} \cdot \omega\left(\frac{r}{a}\right)\ . \tag{2.1.12}$$

The Thomas-Fermi radius of the atom $a = \left(\frac{9}{128}\frac{\pi^2}{Z}\right)^{\frac{1}{3}}$ is also used as a length unit in the substitution $y = \frac{\rho}{a}$. Comparing the derived cross section to Rutherford's scattering law

$$Q_{\text{Ruth}} \;=\; \left(\frac{2\alpha}{k_0}\right)^2 \frac{1}{\chi^4} \tag{2.1.13}$$

the constants

$$\alpha \;=\; \alpha_{\text{sfld}} \frac{zZ}{\beta}\ , \tag{2.1.14}$$

with $\alpha_{\text{sfld}} \approx \frac{1}{137}$ and $\beta = \frac{v}{c}$, and

$$\chi_0 \;=\; \frac{1}{ak_0} \tag{2.1.15}$$

are used. Molière states that the second factor of the ratio

$$q(\chi) \equiv \frac{Q(\chi)}{Q_{\mathrm{Ruth}}(\chi)} = \chi^4 \cdot \left(\frac{1}{4\alpha^2\chi_0^4} \left| \int_0^\infty \mathrm{d}y \; yJ_0\left(y\frac{\chi}{\chi_0}\right)\left[\mathrm{e}^{i\phi(ay)} - 1\right] \right|^2 \right) \tag{2.1.16}$$

can be approximated such that

$$q(\chi) \approx \frac{\chi^4}{(\chi^2 + \chi_a^2)^2} \tag{2.1.17}$$

which is supposed to be sufficiently accurate for the derivation of his theory of multiple scattering (see chap. 2.2). Thus the whole single scattering law is reduced to the determination of only one parameter in (2.1.17): the so called "screening angle" χ_a . A calculation formula is derived by Molière by an interpolation:

$$\chi_a^2 = \chi_0^2(1.13 + 3.76\alpha^2) \; . \tag{2.1.18}$$

In his review, Scott shows that the Molière's resulting multiple-scattering distribution is insensitive to the exact value of χ_a [26].

2.2 Multiple scattering

Molière's approach to describe the multiple scattering of fast charged particles is based on his theory of the single scattering process (see chap. 2.1). In his second "Mitteilung" [16] (engl. message) it is introduced as a summation of incoherent elastic single scatters (each scattering of a particle with one atom is regarded as to be independent of other scatters and atoms).

The probability for a single scattering into the spatial angle element

$$\mathrm{d}\omega(\chi) = 2\pi\sin(\chi)\mathrm{d}\chi \approx 2\pi\chi\mathrm{d}\chi$$

(that equals a scattering angle (see Fig. 1) between χ and χ+dχ) inside of a traversed thickness t (length) can be written as

$$W(\chi)\chi\mathrm{d}\chi \equiv NtQ(\chi)2\pi\chi\mathrm{d}\chi = \frac{2\chi_c^2 q(\chi)}{\chi^4}\chi\mathrm{d}\chi \tag{2.2.1}$$

for small χ , with $q(\chi)$ as in (2.1.17). Here, N is the number of scattering atoms per volume and χ_c the "characteristic angular constant":

$$\chi_c^2 \equiv 4\pi\left(\frac{\alpha}{k_0}\right)^2 Nt \tag{2.2.2}$$

(formulae used for calculations: see chap. 3). Thus the expected number of single scatterings (mean) for particles traversing t is to be defined as the summation of every $\mathrm{d}\omega(\chi)$'s single scattering probability with $\chi > \epsilon$:

$$\Omega_0 \;=\; \lim_{\epsilon\to 0}\int_{\epsilon}^{\infty} W(\chi)\chi\mathrm{d}\chi \tag{2.2.3}$$

(*note:* (2.2.1) is not an angular distribution). Since it is physically reasonable to assume a fast decaying $W(\chi)$, the upper limit of integration (2.2.3) can be set to ∞ for simplification.

In the following, the quantity Ω_0 is only used for formal purposes and will eventually drop out of the result. Its physical significance is limited by the incoherent derivation of $W(\chi)$, which is neglecting overlaps and interactions of different atomic shells in regions that contribute to small χ .

Based on the ansatz chosen by Wentzel in [17], Molière first determines the contribution of each n-times scattering process ($n = 0, 1, 2, ...$) to the overall angular distribution. According to (2.2.1), the probability for no scatterings with the angle χ to occur is given by

$$1 - W(\chi)\chi\mathrm{d}\chi \;\approx\; \mathrm{e}^{-W(\chi)\chi\mathrm{d}\chi} \;. \tag{2.2.4}$$

Thus the probability for a particle traversing t to experience no scattering at all is given by $\prod_{i=1}^{\infty}\exp[-W(\chi_i)\chi_i\mathrm{d}\chi_i] = \mathrm{e}^{-\Omega_0}$ employing (2.2.3).

At this point, the relevant part of the unit ball is again approximated by a tangential plane perpendicular to the incidental direction of the particle (see chap. 2.1). Thus angles θ can be represented by two-dimensional vectors $\vec{\theta}$ in the plane and $\mathrm{d}\omega(\theta) = 2\pi\chi\mathrm{d}\chi$ becomes the area element $\mathrm{d}\sigma_\theta$ (see Fig. 2).

Hence the contribution of passages with no scatterings to the overall angular distribution is

$$f_0(\vec{\theta})\frac{\mathrm{d}\sigma_\theta}{2\pi} \;=\; \mathrm{e}^{-\Omega_0}\delta_2(\vec{\theta})\frac{\mathrm{d}\sigma_\theta}{2\pi} \tag{2.2.5}$$

where $\delta_2(\vec{\theta})$ is the two-dimensional Dirac's δ-distribution ($\iint u(\vec{x})\delta_2(\vec{x})\frac{\mathrm{d}\sigma_x}{2\pi} = u(0)$). The contribution of a single scattering with a deviation of $\vec{\theta}$ in $\mathrm{d}\sigma_\theta$ is

$$f_1(\vec{\theta})\frac{\mathrm{d}\sigma_\theta}{2\pi} \;=\; \mathrm{e}^{-\Omega_0}W(\vec{\theta})\frac{\mathrm{d}\sigma_\theta}{2\pi} \tag{2.2.6}$$

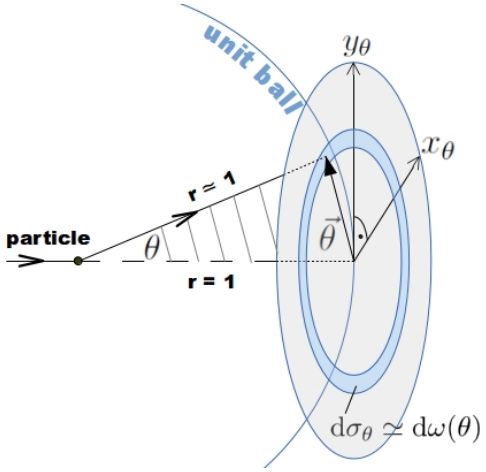

Figure 2: Small θ can be replaced by vectors $\vec{\theta}$ in the plane approximating the dominating angular range (*grey*); the plane element $\mathrm{d}\sigma_\theta$ replaces the spatial angle intervall $\mathrm{d}\omega(\theta)$

which leads to a recursion formula for

$$f_n(\vec{\theta}) \;=\; \frac{1}{n}\iint\limits_{\mathbb{R}^2} f_{n-1}(\vec{\theta}-\vec{\chi})W(\vec{\chi})\frac{\mathrm{d}\sigma_\theta}{2\pi}\;. \tag{2.2.7}$$

The $\frac{1}{n}$-factor ensures that each possible combination of n single scatters accumulating to $\vec{\theta}$ is only counted once regardless of their order.

Now these functions are to be represented by Hankel transformations (two-dimensional Fourier transformations of radial symmetric functions with Bessel functions as the basis). Their properties allow one to perform a convolution on the Hankel integrals u_1 and u_2

$$u_{1/2}(\vec{c}) \;=\; \int\limits_0^\infty v_{1/2}(y)J_0(xy)y\mathrm{d}y$$

such that

$$\iint\limits_{\mathbb{R}^2} u_1(\vec{x}-\vec{w})u_2(\vec{w})\frac{\mathrm{d}\sigma_w}{2\pi} \;=\; \int\limits_0^\infty v_1(y)v_2(y)J_0(xy)y\mathrm{d}y\;. \tag{2.2.8}$$

Thus, using

$$p(\chi)\chi \mathrm{d}\chi \equiv \chi \mathrm{d}\chi \int_0^\infty \Omega(y) J_0(\chi y) y \mathrm{d}y \ , \tag{2.2.9}$$

$$\delta_2(\vec{x}) = \int_0^\infty J_0(xy) y \mathrm{d}y \tag{2.2.10}$$

and a successive elimination of f_{n-1} , f_{n-2} etc., Eqn. (2.2.7) transforms into

$$f_n(\theta) = \mathrm{e}^{-\Omega_0} \int_0^\infty \frac{\Omega(y)^n}{n!} J_0(\theta y) y \mathrm{d}y \ . \tag{2.2.11}$$

With the new introduced function $\Omega(y)$, that is obtained by conversion of (2.2.9):

$$\Omega(y) = \int_0^\infty J_0(\chi y) W(\chi) \chi \mathrm{d}\chi \ , \tag{2.2.12}$$

the overall angular distribution is the sum of all contributing $f_n(\theta)$:

$$f(\theta)\theta \mathrm{d}\theta = \theta \mathrm{d}\theta \int_0^\infty \mathrm{e}^{\Omega(y)-\Omega_0} J_0(\omega y) y \mathrm{d}y \ . \tag{2.2.13}$$

In chap. 2.1 , an approximate expression for the ratio $q(\chi)$ was derived (see (2.1.17)). Hence the mean number of scatterings as defined in (2.2.3) results in $\Omega_0 = \frac{\chi_c^2}{\chi_a^2}$. Thus (2.2.12) can be written as

$$\Omega(y) = 2\Omega_0 \int_0^\infty \frac{J_0\left(\xi y \chi_a\right)}{\left(1+\xi^2\right)^2} \xi \mathrm{d}\xi \tag{2.2.14}$$

with $\xi = \frac{\chi}{\chi_a}$. Here, the integral is to be expanded as a power series and the substitution $y' \equiv y\chi_c$ is used such that the exponent in (2.2.13) can be approximated by

$$\Omega(y') - \Omega_0 = \left(\frac{y'}{2}\right)^2 \ln\left(\frac{\mathrm{e}^{2C-1}}{\Omega_0}\left(\frac{y'}{2}\right)^2\right) + \frac{1}{2\Omega_0}\left(\frac{y'}{2}\right)^4 \ln\left(\frac{\mathrm{e}^{2C-2.5}}{\Omega_0}\left(\frac{y'}{2}\right)^2\right) + \cdots \tag{2.2.15}$$

$$\approx \frac{y'^2}{4}\left(\ln\frac{y'^2}{4} - b\right) \tag{2.2.16}$$

($C = 0.5772...$: Euler–Mascheroni constant). Here, the neglection of terms of second order and higher is justified for large Ω_0 as it is expected in the case of multiple scattering.

To simplify later series expansions, the parameter b is substituted by introducing the quantity B, for which holds true for

$$b \;=\; 1 - 2C + \ln\frac{\chi_c^2}{\chi_a^2} \;\equiv\; B - \ln B \;. \tag{2.2.17}$$

Using the approximation (2.2.16) and applying the substitution $y = y'\sqrt{B}$ distribution (2.2.13) transforms into

$$f(\theta)\theta\mathrm{d}\theta \;=\; \frac{\theta\mathrm{d}\theta}{\chi_c^2 B}\int_0^\infty \mathrm{d}y\; yJ_0\left(\frac{\theta}{\chi_c\sqrt{B}}y\right)\mathrm{e}^{-\frac{y^2}{4}}\cdot\exp\left[\frac{1}{B}\frac{y^2}{4}\ln\frac{y^2}{4}\right] \;. \tag{2.2.18}$$

Since for the current issue a projected scattering angle ϕ is required, distribution (2.2.18) is to be transformed. Therefore, an integration of (2.2.18) over ψ - an angle in in a plane perpendicular to the projection plane of ϕ - from $-\infty$ to ∞ is performed. This gives

$$f(\phi)\mathrm{d}\phi \;=\; \frac{\mathrm{d}\phi}{\pi\chi_c\sqrt{B}}\int_0^\infty \mathrm{d}y\;\cos\left(\frac{\phi}{\chi_c\sqrt{B}}y\right)\mathrm{e}^{-\frac{y^2}{4}}\cdot\exp\left[\frac{1}{B}\frac{y^2}{4}\ln\frac{y^2}{4}\right] \tag{2.2.19}$$

which is already normalized such that $\int\limits_{-\infty}^{\infty} f(\phi)\mathrm{d}\phi = 1$.

Expanding the second exponential function in (2.2.19) as a Taylor series the distribution becomes

$$f(\varphi)\mathrm{d}\varphi \;=\; \frac{\mathrm{d}\varphi}{\sqrt{\pi}}\left[\mathrm{e}^{-\varphi^2} + \frac{1}{B}f^{(1)}(\varphi) + \frac{1}{B^2}f^{(2)}(\varphi) + \cdots\right] \tag{2.2.20}$$

with

$$f^{(n)}(\varphi) \;=\; \frac{1}{n!\sqrt{\pi}}\int_0^\infty \mathrm{d}y\;\cos(\varphi y)\mathrm{e}^{-\frac{y^2}{4}}\cdot\left[\frac{y^2}{4}\ln\frac{y^2}{4}\right]^n \tag{2.2.21}$$

using a reduced angle variable

$$\varphi \;=\; \frac{\phi}{\chi_c\sqrt{B}} \;.$$

Since $\int\limits_{-\infty}^{\infty} f^{(n)}(\varphi)\mathrm{d}\varphi = 0$ for $n \geq 1$, the norm is conserved in (2.2.20) and the normalization equals the one of the gaussian term in zeroth order.

From here on, only the gaussian, first and second order term of the expansion in (2.2.20) are considered. These are sketched in Fig. 3 . In chap. 3 all parameters necessary for the actual evaluation of the distribution function are summarized and the particular implementation is described. Furthermore, power series and asymptotic formulae for the calculation of $f^{(1)}(\varphi)$ and $f^{(2)}(\varphi)$ are given.

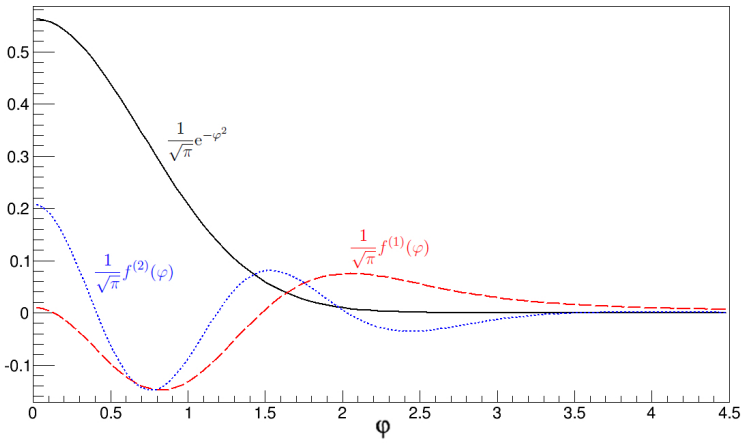

Figure 3: Sequence members of Molière's series expansion for the scattering angle distribution $f^{(n)}(\varphi)$ up to the second order.

2.3 Highland's approximation

Since the dominating contribution to Molière's distribution is gaussian-like (see Eqn. (2.2.20)), it is straightforward to propose a gaussian approximation to it.

In 1941, Rossi and Greisen derived a small angle multiple elastic scattering law [27] from Rutherford's single scattering law for singly charged projectile particles. Assuming a gaussian distribution, they integrated the mean square angle of a scattering process according to (2.1.13) over the thickness t and obtained the standard deviation

$$\theta_{\text{Rossi}} = \frac{10.6 \text{ MeV}}{\beta cp}\sqrt{\frac{\rho t}{X_0}} \tag{2.3.1}$$

(p : momentum of the scattered particle, X_0 : radiation length, see 3) for the projected angle distribution. Starting from here on, Highland semi-analytically modified formula (2.3.1) by introducing a correction term and deriving constants from a data fit [28]. Because its predictions were only in good agreement with measurements for atoms with $Z \approx 47$ (silver) and since there was an incorrect modification employed in the theory, Highland's formula was later revised by Lynch and Dahl [22]. Fits of gaussians to the central 98% of Molière's distribution lead to a better result for all Z .

Thus, the RMS angle (in rad)

$$\theta_0 = \frac{13.6 \text{ MeV}}{\beta cp}\sqrt{\frac{\rho t}{X_0}}\left[1 + 0.088 \cdot \log_{10}\left(\frac{\rho t}{X_0}\right)\right] \tag{2.3.2}$$

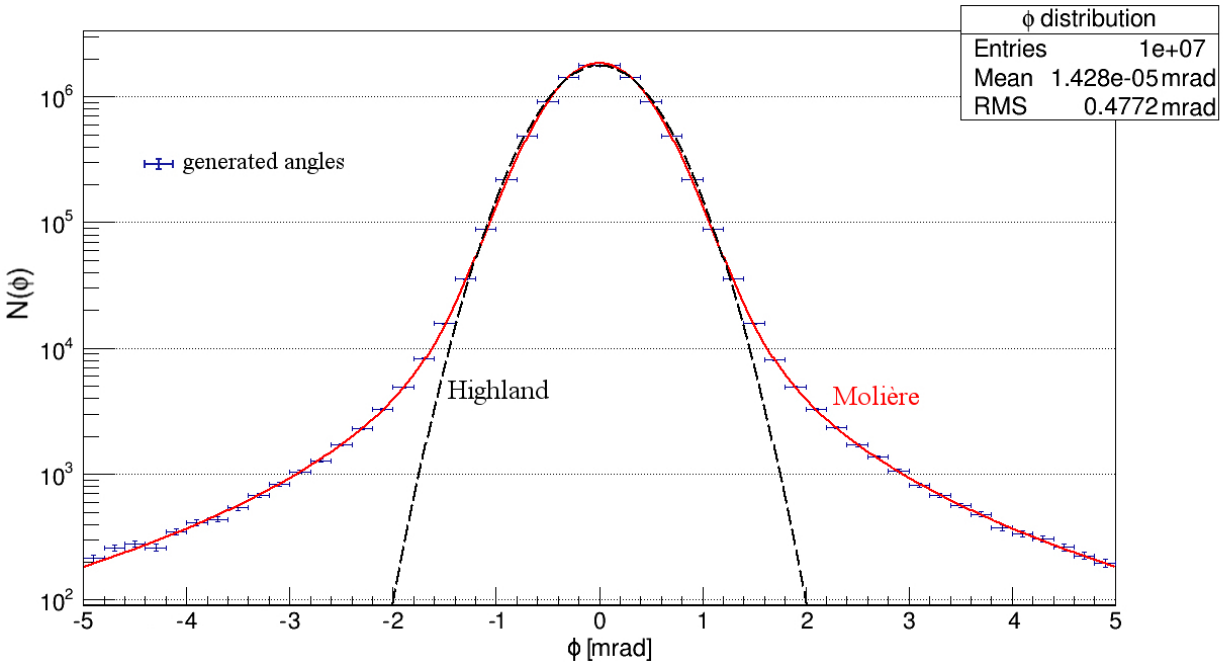

Figure 4: Comparison of Molière's angular distribution ($\sqrt{\frac{\chi_c^2 B}{2}} = 0.433$ mrad) for muons with $p_\mu = 100$ GeV after traversing 1 m "Fréjus rock" (see [6]) with its Highland approximation ($\theta_0 = 0.452$ mrad). The random angles are generated as described in chap. 3.3 .

characterizes the probability distribution of the projected angle θ :

$$f(\theta)\mathrm{d}\theta \;=\; \frac{1}{\sqrt{2\pi}\theta_0}\mathrm{e}^{-\frac{\theta^2}{2\theta_0^2}}\mathrm{d}\theta. \tag{2.3.3}$$

Highland's approximation in comparison with Molière's distribution is pictured in Fig. 4 .

3 Calculation and implementation

In the following, the actual formulae used for computing the distribution functions and their implementation for PROPOSAL are described. Furthermore, methods are pointed out that can be used when dealing with not just one-atomic materials, but compounds and mixtures.

Since the use of different conventions of units can cause a lot of confusion while reading various literature and performing actual calculations, dimensions of quantaties are explicitly presented. In general, the SI system of units is used. Some values of constant factors have been roughly calculated as well. The results have been doublechecked for validity.

3.1 Molière

As stated in chap. 2.1 , Molière's single scattering law can be reduced to the determination of the screening angle χ_a . Using the angular constant

$$\chi_0 = \frac{1}{ak_0} = \alpha_{\text{sfld}} \left(\frac{128}{9\pi^2} Z\right)^{\frac{1}{3}} \frac{m_e c}{p} \approx 4.212 \cdot 10^{-3} \frac{Z^{1/3}}{p[\text{MeV/c}]} \text{ rad} \tag{3.1.1}$$

(m_e : rest mass of an electron, p momentum of the scattered particle) it is calculated as given in (2.1.18). Here and in the following, the velocity

$$\beta = \frac{v}{c} = \frac{1}{\sqrt{1 + \frac{m^2 c^2}{p^2}}} \tag{3.1.2}$$

entering $\alpha = \alpha_{\text{sfld}} \frac{zZ}{\beta}$ is the only parameter differentiating between different leptonic generations by the rest mass m of the scattered particle.

To describe the multiple scattering law, only the characteristic angular constant χ_c is additionally required.
Often a modification proposed by Bethe in [23] is applied to (2.2.2) by employing the correction factor $\frac{Z+1}{Z}$ to take into account the scatterings by atomic electrons. Scott [26] and Butkevich et al [21] already argued that this is not appropiate for "heavy particles" like muons. Comparisons to measurement data by Attwood et al [29] show a better agreement for elements with small Z with Molière's distribution using Z^2 rather than $Z(Z+1)$ in χ_c^2 . For higher Z both distributions become almost indistinguishable. Hence Bethe's modification is to be chosen here only for electrons. For other particles, χ_c is evaluated according to

$$\chi_c^2 = 4\pi\hbar^2 \alpha_{\text{sfld}}^2 N_{\text{A}} \cdot \frac{Z^2 \rho}{A} \frac{t}{\beta^2 p^2} \ . \tag{3.1.3}$$

in rad^2 . Here the number of atoms per volume N in (2.2.2) has been replaced by $\frac{N_A \rho}{A}$ where ρ is the density in g/cm^3 , A the molar mass in g/mol and N_A Avogadro's number in mol^{-1} . Inserting t in cm and p in MeV/c the constant factor results in ~ 0.1569 .

Having calculated χ_a and χ_c , the parameter B can be derived by solving Eqn. (2.2.17). Since there is no analytical solution to it, this is done by means of a Newton-Raphson method with an inital guess $B_0 = 15$ (this is stable, because $\ln B - B$ has only one minimum at $B = 1$ where it is 0). In [16] Molière gives a lower limit for the validity of his theory at $B \approx 4.5$ ($\rightarrow \Omega_0 = \chi_c^2/\chi_a^2 \approx 23$). Since this only occurs for very small densities ρ or flight distances t (maybe in combination with a very high Z), it is practical and reasonable to set $f(\phi)\mathrm{d}\phi = \delta(\phi)\mathrm{d}\phi$ (Dirac's $\delta \rightarrow$no deviation) in that case.

In his original paper [16], Molière gives power series expansions for the expansion terms $f^{(1)}(\varphi)$ and $f^{(2)}(\varphi)$ in (2.2.20):

$$\begin{aligned} f^{(1)}(\varphi) &= \sum_{p=0}^{\infty} \frac{(-1)^p}{p!} \left(p + \frac{1}{2}\right) \psi(p + \frac{3}{2}) \cdot \varphi^{2p} \ , && (3.1.4) \\ &\approx 0.018245 - 1.0547\varphi^2 + 1.3789\varphi^4 - \cdots \ , \\ f^{(2)}(\varphi) &= \sum_{p=0}^{\infty} \frac{(-1)^p}{p!} \binom{p + \frac{3}{2}}{2} \left[\psi^2(p + \frac{5}{2}) + \psi_1(p + \frac{5}{2})\right] \cdot \varphi^{2p} \ , && (3.1.5) \\ &\approx 0.36830 - 2.9012\varphi^2 + 4.7637\varphi^4 - \cdots \end{aligned}$$

where $\psi(z)$ is the digamma function. For the evaluation of the trigamma function $\psi_1(z)$, the algorithm of Schneider [30] was implemented and modified to obtain a higher precision. The generalized binomial coefficient in (3.1.5) (also valid for noninteger arguments) is supposed to be computed as

$$\binom{x}{y} = \frac{\Gamma(x+1)}{\Gamma(y+1)\Gamma(x-y+1)} \qquad (3.1.6)$$

with the gamma function $\Gamma(z)$.
Since both power series are slowly convergent, their first 70 coefficients have been tabulated, so that the polynominals can be evaluated by use of Horner's scheme.

To avoid numerical errors in the case of larger φ , the asymptotic formula

$$\begin{aligned} f^{(1)}(\varphi) &\approx \frac{\sqrt{\pi}}{2} \sum_{p=1}^{\infty} \frac{p}{2^{p-1}} (2p-1)!! \cdot \left|\varphi^{-(2p+1)}\right| && (3.1.7) \\ &\approx \frac{\sqrt{\pi}}{2} \frac{1}{|\varphi^3| \left(1 - \frac{9}{2}\varphi^{-2}\right)^{\frac{2}{3}}} && (3.1.8) \end{aligned}$$

(with the double factorial $k!! = k(k-2)(k-4)\ ...$) is only applied for $\varphi^2 > 12$. It is derived by expanding the $\mathrm{e}^{-\frac{y^2}{4}}$ in (2.2.21). Following the relation

$$I(p) \;=\; \int_0^\infty \mathrm{d}y\, \cos(\varphi y) \left(\frac{y^2}{4}\right)^p \;=\; \sqrt{\pi}\frac{\Gamma(p+\frac{1}{2})}{\Gamma(-p)} \cdot \varphi^{-(2p+1)} \tag{3.1.9}$$

given in [16] using the differentiations with respect to p

$$\frac{\mathrm{d}^n}{\mathrm{d}p^n} I(p) \;=\; \int_0^\infty \mathrm{d}y\, \cos(\varphi y) \left(\frac{y^2}{4}\right)^p \left(\ln\frac{y^2}{4}\right)^n \tag{3.1.10}$$

this leads to series expansions for $f^{(1)}(\varphi)$ and $f^{(2)}(\varphi)$. The first one results in the same solution that Molière summarized to (3.1.8). For the second expansion series, the obtained outcome

$$f^{(2)}(\varphi) \;\approx\; \frac{\sqrt{\pi}}{2} \sum_{p=2}^{\infty} p(p-1)\frac{(2p-1)!!}{2^{p-2}} \left(\frac{C}{2} + \ln(2|\varphi|) - \sum_{k=0}^{p-1}\frac{1}{2k+1}\right) \cdot \left|\varphi^{-(2p+1)}\right| \tag{3.1.11}$$

is not equivalent to Molière's result. Unfortunately, in his original paper [16] the calculations were not discussed in detail. Given its consistency, with results from (3.1.4), series (3.1.11) is regarded as to be correct and used from $\varphi = \pm 4.25$ on with $p = 2, 3, ...12$.

In case of a compound medium with n components, the characteristic angle χ_c (cf. (3.1.3)) is calculated with an average A and Z^2 . Using the mass fraction

$$w_i \;=\; \frac{k_i A_i}{\sum\limits_{j=1}^{n} k_j A_j} \tag{3.1.12}$$

(k_i : number of atoms of the ith component per compound unit cell/molecule) it is given by

$$\chi_c^2 \;=\; 4\pi\hbar^2\alpha_{\mathrm{sfld}}^2 \cdot \frac{\rho t}{\beta^2 p^2} \cdot \left(\sum_{i=1}^{n} w_i Z_i^2 \Big/ \sum_{j=1}^{n} w_j A_j\right) \;. \tag{3.1.13}$$

Thus the parameter B is computed (as in (2.2.17)) for each component with the respective χ_a . As also suggested in [21], the resulting angular distribution is to be defined as the arithmetic mean of the distributions for each component $f_i(\varphi_i = \phi/\chi_c\sqrt{B_i})\mathrm{d}\varphi_i$ weighted by $w_i Z_i^2$:

$$f(\varphi)\mathrm{d}\varphi \;=\; \frac{\sum\limits_{i=1}^{n} w_i Z_i^2 f_i(\varphi_i)\mathrm{d}\varphi_i}{\sum\limits_{j=1}^{n} w_j Z_j^2} \;. \tag{3.1.14}$$

3.2 Highland

While calculating the decisive θ_0 after (2.3.3), again the only parameter distinguishing different projectile particles is the velocity factor β (cf. (3.1.2)). All information about the scattering medium are contained in its radiation length X_0 ($[X_0] = 1$ g/cm^2). It is defined as the mean distance one electron passes within the medium until it has emitted all but e^{-1} of its initial energy by bremsstrahlung. As described in [31], it is to be computed using Tsai's formula [32]

$$\frac{1}{X_0} \;=\; \frac{4\alpha_{\text{sfld}} r_e^2 N_{\text{A}}}{A} \left(Z^2 [L_{\text{rad}} - f(Z)] + Z L'_{\text{rad}} \right) \;. \tag{3.2.1}$$

In (3.2.1), with the classical electron radius $r_e = 2.82 \cdot 10^{-13}$ cm , the constants can be summarized to $4\alpha_{\text{sfld}} r_e^2 N_{\text{A}} \approx 1,396 \cdot 10^3$ cm^2/mol .

For elements up to uranium ($Z = 92$), the Coulomb correction can be approximated by

$$f(Z) \;=\; a^2 \left[(1+a^2)^{-1} + 0.20206 - 0.0369 a^2 + 0.0083 a^4 - 0.002 a^6 \right] \tag{3.2.2}$$

($a \equiv \alpha_{\text{sfld}} Z$) with good accuracy [33]. The radiation logarithms L_{rad} and L'_{rad} are tabulated in Tab. 1 .

Table 1: Best estimates for the radiation logarithms L_{rad} and L'_{rad} by Tsai [32].

Element	Z	L_{rad}	L'_{rad}
H	1	5.31	6.114
He	2	4.79	5.621
Li	3	4.74	5.805
Be	4	4.71	5.924
others	$\geq$5	$\ln(184.15 \cdot Z^{-\frac{1}{3}})$	$\ln(1194 \cdot Z^{-\frac{2}{3}})$

If a medium contains more than one element, the overall radiation length is approximated by a weighted sum

$$\frac{1}{X_0} \;=\; \sum_{i=1}^{n} \frac{w_i}{X_{0,i}} \;=\; \frac{\sum\limits_i k_i A_i / X_{0,i}}{\sum\limits_j k_j A_j} \tag{3.2.3}$$

over all single atomic components i that appear k_i times per molecule/unit cell (w_i : mass fraction).

An implementation following exactly the scattering parameter formulae described above has replaced the current implementation in PROPOSAL. The older implementation was unnecessarily complicated. Furthermore, an incorrect derivation of the radiation length X_0 lead to distinctly inaccurate results for θ_0 for all particles, but electrons (values about a factor $\sim 10^3$ to small for muons, compare Fig. 9 and 10). To take into account (smaller) particle momenta for muons around ~ 1 GeV/c (cf. $m_\mu \approx 0.1$ GeV/c^2) the velocity β had to be introduced. It was set to 1 in the former implementation of Eqn. (2.3.3).

3.3 Generating random numbers

Scattering angles following the gaussian Highland distribution were generated by PROPOSAL using the method StandardNormal [6]. StandardNormal is transforming uniformly distributed random numbers using several integration methods. Thus, it is easier and faster to generate random angles θ by comparing uniformly distributed random variables $X \in (-0.5, 0.5)$ to the indefinite integral of (2.3.3)

$$F(\theta) \;=\; \frac{1}{\sqrt{2\pi}\theta_0} \int \mathrm{e}^{-\frac{\theta^2}{2\theta_0^2}} \mathrm{d}\theta \;=\; \frac{1}{2}\mathrm{erf}\left(\frac{\theta^2}{\sqrt{2}\theta_0}\right) \tag{3.3.1}$$

(cf. Fig. 5), where $\mathrm{erf}(x)$ is the error function. The angle θ that satisfies $X = F(\theta)$ is given by the inversion of (3.3.1)

$$\theta \;=\; (\sqrt{2}\theta_0) \cdot \mathrm{erf}^{-1}(2X) \tag{3.3.2}$$

making use of the inverse error function $\mathrm{erf}^{-1}(x)$. The advantage of this method in terms of computation speed is shown in chap. 4.3 .

Molière distributed angles are supposed to be produced in a similar way (see Fig. 5). Since Molière's function is not a mere gaussian, its indefinite integral $F(\phi)$ can not be inversed as easily as the one of Highland's function.

Hence, the respective angle ϕ where $X = F(\phi)$ is to be evaluated using the Newton-Raphson method

$$\phi_{n+1} \;=\; \phi_n - \frac{F(\phi_n) - X}{f(\phi_n)} \;. \tag{3.3.3}$$

The iteration is to be performed until ϕ_{n+1} is exact to at least four decimals. To fasten the computation speed, the inverse error function is used for estimating the initial value $\phi_0 \;=\; (\chi_c\sqrt{B})\cdot\mathrm{erf}^{-1}(2X)$. A result of the described method is shown in Fig. 4 .

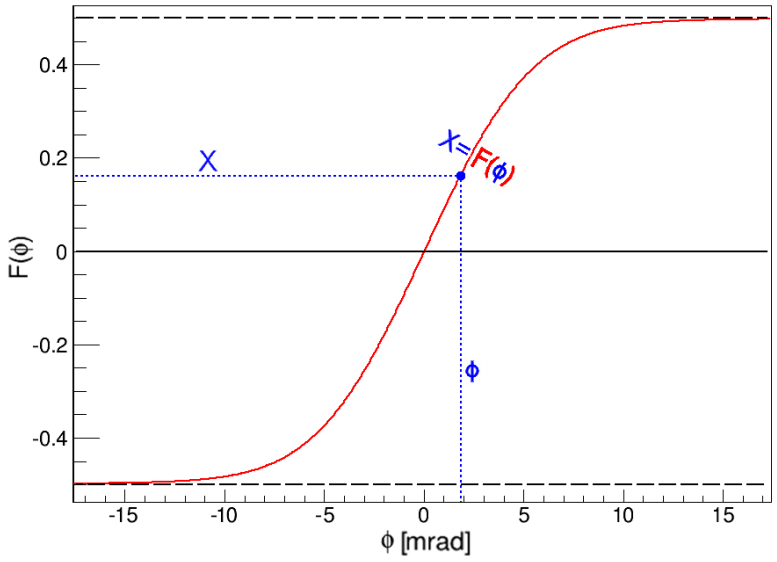

Figure 5: Generating random angles ϕ in compliance with Highland's or Molière's distribution from uniformly distributed X : determine the point of intersection of X and the integral $F(\phi)$.

Therefore, distribution (2.2.20) is to be integrated:

$$F(\varphi) \;=\; \int f(\varphi)\mathrm{d}\varphi \;=\; \frac{1}{\sqrt{\pi}}\left[\frac{\sqrt{\pi}}{2}\mathrm{erf}(\varphi) + \frac{1}{B}F^{(1)}(\varphi) + \frac{1}{B^2}F^{(2)}(\varphi)\right] \;. \tag{3.3.4}$$

The indefinite integrals of the expansion terms

$$F^{(n)}(\varphi) \;=\; \int f^{(n)}(\varphi)\mathrm{d}\varphi \;,\; n = 1, 2 \tag{3.3.5}$$

are computed as integrals of the respective series representations for smaller reduced angles φ (see Eqn. (3.1.4) & (3.1.5))

$$F^{(1)}(\varphi) \;=\; \sum_{p=0}^{\infty} \frac{(-1)^p}{(2p+1)p!}\left(p+\frac{1}{2}\right)\psi(p+\frac{3}{2})\cdot\varphi^{2p+1} \;, \tag{3.3.6}$$

$$F^{(2)}(\varphi) \;=\; \sum_{p=0}^{\infty} \frac{(-1)^p}{(2p+1)p!}\binom{p+\frac{3}{2}}{2}\left[\psi^2(p+\frac{5}{2}) + \psi_1(p+\frac{5}{2})\right]\cdot\varphi^{2p+1} \tag{3.3.7}$$

employing Horner's scheme (p up to 69) and larger φ (see Eqn. (3.1.7) & (3.1.5))

$$F^{(1)}(\varphi \geq \varphi_{(1)}) = -\mathrm{sgn}(\varphi)\frac{\sqrt{\pi}}{2}\sum_{p=1}^{\infty}\frac{(2p-1)!!}{2^p}\cdot\varphi^{-2p}\ , \tag{3.3.8}$$

$$F^{(2)}(\varphi \geq \varphi_{(2)}) = -\mathrm{sgn}(\varphi)\frac{\sqrt{\pi}}{2}\sum_{p=2}^{\infty}(p-1)\frac{(2p-1)!!}{2^{p-1}} \cdot\left(\frac{C}{2}+\ln(2|\varphi|)+\frac{1}{2p}-\sum_{k=0}^{p-1}\frac{1}{2k+1}\right)\cdot\varphi^{-2p}\ . \tag{3.3.9}$$

Here, again the summation is performed up to $p = 12$. The boundary angles $\varphi^2_{(1)} = 12$ and $\varphi^2_{(2)} = 18$ have been chosen in a way such that the junctions of both parametrizations are close to the points where (3.3.6) and (3.3.7) become numerical instable (start to diverge). In order to keep it continuous, the crossover for $F^{(2)}(\varphi)$ was slightly smoothed by a parabola.

4 Validation

4.1 Comparison with measurement data

In order to examine the validity of theories and algorithms described in former chapters, their outcome is to be checked against measurement data (see Fig. 7). Therefore, data of Akimenko et al [34] is used who measured the deviation of 7.3 GeV/c muons traversing 1.44 cm (≈ 1 rad. length) of copper.

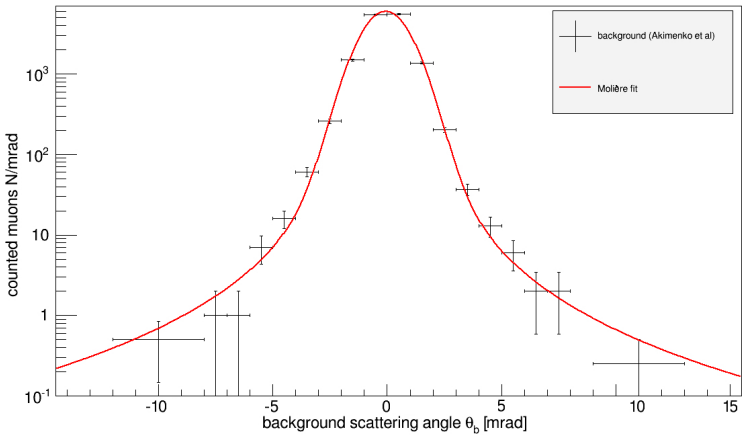

Figure 6: Background deviation distribution caused by the measurement setup of Akimenko et al [34] (14484 muons, $p_\mu = 7.3$ GeV/c). Approximation by a Molière's function.

Due to properties of the experimental set up, the measured distribution is affected by "background deviations" coming scatterings outside of the copper target and errors of the track reconstruction. Hence, measurements without the target were performed that lead to the distribution displayed in Fig. 6 . A Molière's function $f(\theta_b)$ with $\chi_c^2 = 8.7562 \cdot 10^{-8}$ rad^2 , $B = 21.435$ and a mean at -0.07 mrad is used for generating background events, since it is approximating the distribution's shape decently, which is considerably referable to multiple scatterings inside of a scintillation detector in front of the target.
In this way, a Monte Carlo simulation combines random scattering angles θ and random background angles θ_b to the resulting total scattering angle θ_t . Thus obtained data is shown in Fig. 7 . Here, the RMS angle of Highland's approximation is $\theta_0 = 1.863$ mrad (cf. $\sqrt{\chi_c^2 B/2} = 1.888$ mrad).
The deviation plot Fig. 8 shows that Molière's theory is in good agreement with the measured data up to ca. $4.5 \cdot \theta_0$, whereas Highland's formula is only applicable up to less than $2 \cdot \theta_0$. As already shown in [29], Molière's distribution is overestimating the probability for larger angles, but still allows a satisfactory description, since less

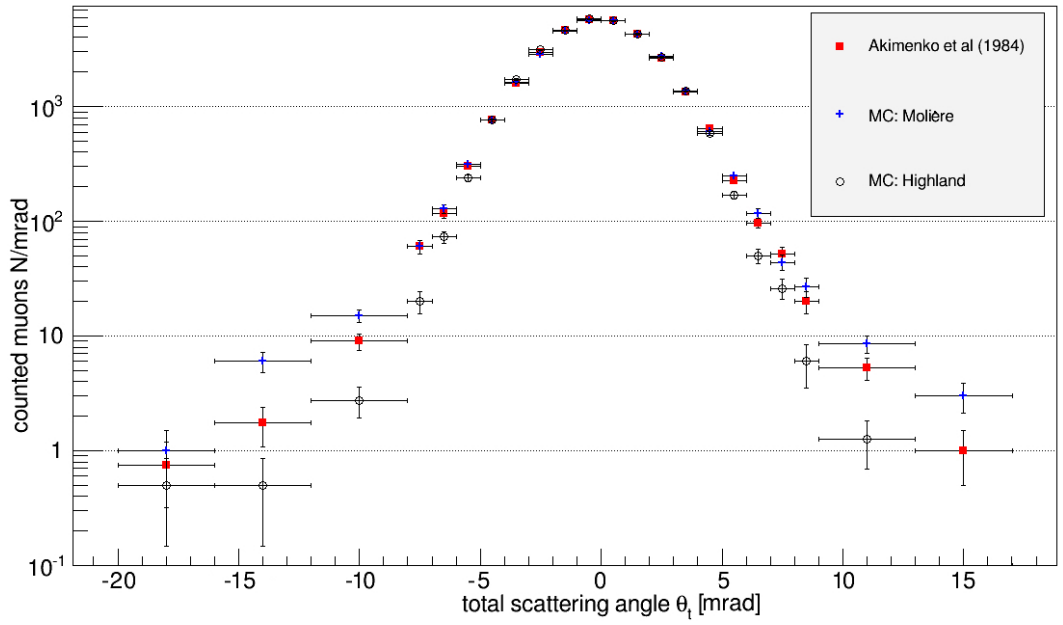

Figure 7: Measurement data of 31125 scattered muons compared with Monte Carlo simulations employing Molière's scattering law and Highland's formula as implemented for PROPOSAL.

than 0.5% of the simulated angles were in the region $|\theta| > 4.5 \cdot \theta_0$. In contrast to that, Highland's approximation is crucially underestimating the occurrence of larger angles: The number of measured events with $|\theta| > 3.2 \cdot \theta_0$ is 2.1 times greater than predicted. From here on the background (see Fig. 6) is the dominant contribution in the Monte Carlo simulation employing Highland's formula (Fig. 7). A similiar comparison between both prediction gives a factor of 2.6 .

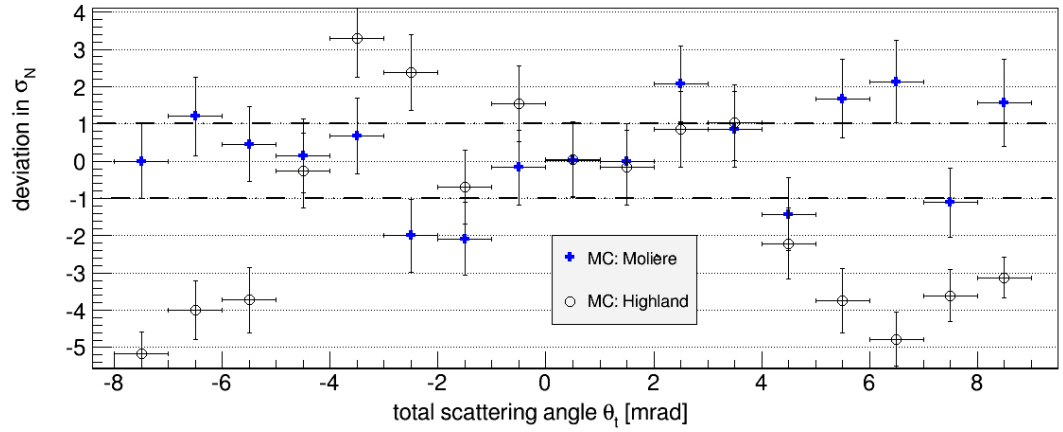

Figure 8: Deviation of the Monte Carlo data from the measurement in terms of the measuring error σ_N .

4.2 Comparison of both parametrizations

In chap. 4.1 , Molière's distribution gave a good describtion for about 99.5% of the measurement data for 7.3 GeV/c muons. Considering a gaussian distribution, 99.5% equals a radius of $\sim 2.807 \cdot \theta_0$. Examining the ratios of the radii of the Molière and Highland parametrization containing 99.5% of the area under the curves, it can be seen that it is almost independent of the particle's momentum, but fastly converging to the values presented in Tab. 2 (the difference of the ratio for $p = 106$ MeV/c and the asymptotic ratio is smaller than +0.06). It is obvious that the ratio is decreasing, but still signifi-

Table 2: Radii of Molière's distribution containing 99.5% of the area under the curve divided by the corresponding radii of Highland's approximation covering the same area for different travel distances t and media (as in [6]).

	1 cm	10 cm	1 m	10 m	100 m	1 km
water	1.58	1.46	1.36	1.28	1.22	1.16
ice	1.58	1.46	1.37	1.29	1.22	1.16
standard rock	1.52	1.41	1.33	1.25	1.19	1.14
salt (NaCl)	1.59	1.47	1.38	1.31	1.24	1.19
copper	1.54	1.44	1.36	1.29	1.23	1.18
lead	1.63	1.53	1.45	1.38	1.32	1.27
uranium	1.63	1.53	1.45	1.38	1.33	1.28

cant, for longer travel distances. The main difference between both multiple scattering parametrizations is that the gaussian approximation is virtually not producing angles in the region dominated by the Molière tail ($f^{(1)}(\varphi)/B + f^{(2)}(\varphi)/B^2$ in Eqn. (2.2.20)). Thus it is suppressing the generation of larger angles. This can become noticable since large amounts of data are necessary for Monte Carlo chains of experiments like IceCube.

In [6] a plot is presented that shows the deviation of 10 TeV/c muons traversing 5 km of ice (see Fig. 9). This plot has been reconstructed using the two newly implemented multiple scattering algorithms (see Fig. 10). Since both plots are based on the same uniformly distributed randomnumbers, the characterisitical differences between both algorithms become obvious:
By comparison, the Highland parametrization leads to larger deviations for trajectories that are mostly affected by medium-angle scatterings. The tail of Molière's function reduces the occurence of scatterings in the medium-angle region in favor of small and large scatterings (cf. Fig. 4). Hence, the larger deviations, which result mainly from one large-angle scatter, are distinctly more prominent. To take into account the overestimation of the probabilities for large-angle events by the Molière-based algorithm, it might be handy to introduce a cut-off angle. It should be chosen regarding the respective experiment's properties and measurement accuracy.

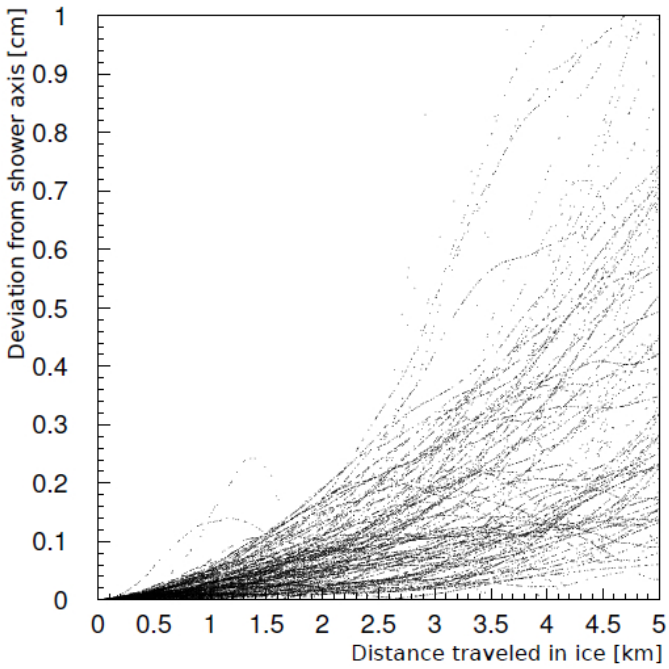

Figure 9: Deviation of 100 muons with $p = 10$ TeV/c traversing 5 km of ice computed by the old version of PROPOSAL [6].

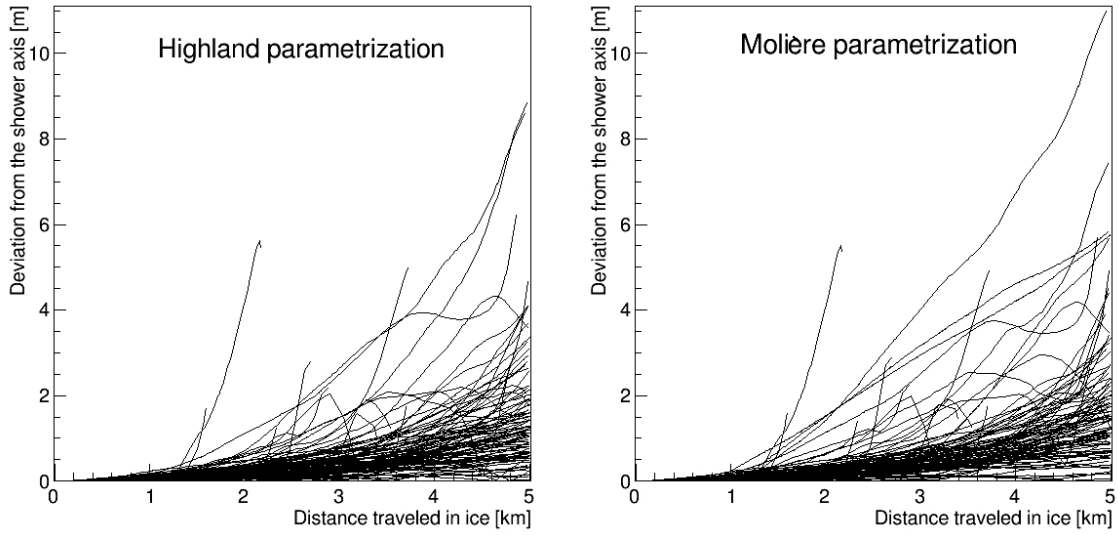

Figure 10: 100 muons ($p = 10$ TeV/c) were propagated with PROPOSAL employing the newly introduced multiple scattering parametrizations. Note that the y-axis is now scaled in meters when comparing to the old incorrect implementation presented in Fig. 9 .

4.3 Computation speed

In order to compare the computation speeds of different algorithms, 10^5 scatters have been performed with each of them while measuring the computation time. A Highland-based algorithm using the old StandardNormal function is to be compared with one applying the new method of random number generation (see 3.3) and the new Molière algorithm. The means of 100 of this measuring cycles for three different media are presented in Tab. 3 .

Table 3: Computation time T in seconds required by different algorithms for the computation of multiple scatterings of 10^5 muons with $p = 10$ TeV/c that traversed 10 m of Fréjus rock, ice or ANTARES water (see [6]).

$T/10^5$ muons in s	Fréjus rock	ice	ANTARES water
Highl. StdNormal	8.186 ± 0.001	8.185 ± 0.001	8.1879 ± 0.0009
Highland new	0.2004 ± 0.0004	0.2007 ± 0.0004	0.2019 ± 0.0004
Molière	2.2746 ± 0.0007	4.2728 ± 0.0007	17.651 ± 0.001

Computations and time measuring have been performed on a laptop computer employing an *Intel® Centrino® 2 vPro™* CPU. The values in Tab. 3 are obviously not generalizable, since test runs on a faster computer system configuration lead to crucially smaller computation times for the algorithm using StandardNormal, so that it is even slightly faster than the Molière algorithm for scatterings in ice. The Highland method applying the new random generator, however, was still by far the fastest algorithm.

Yet it is obvious that the Highland algorithms are almost equally fast for all different media, whereas the Molière parametrization is extremely sensitive to a medium's number of components. In PROPOSAL the medium "Fréjus rock" is treated as a one-atomic medium with an averaged density, atomic mass and nuclear charged [6]. "ANTARES water" again is containing eight components. Thus, the method of averaging the radiation lengths in the case of multi-component media (cf. chap. 3.2) turns out to be extremely timesaving. In contrast to that, the Molière algorithm is basically performing a full scattering calculation for each component, since it is averaging χ_c^2 , $f(\varphi)$ and $F(\varphi)$ (see chap. 3.1 and 3.3). Thus, a scattering computation in "ANTARES water" is lasting almost eight times the computation time of a scattering in "Fréjus rock" for it is involving eight times as many components.

Comparing both Highland algorithms, the new random number method is clearly the one to favor. It is much faster (cf. Tab. 3) and turns out to be even more stable for inserted uniformly distributed random numbers that are very close to 0 or 1 . Apart from these boundaries, both algorithms give the same return values.

5 Conclusion and prospect

5.1 Conclusion

The revision of the multiple scattering algorithm in PROPOSAL resulted in a reimplementation of a simplified and corrected new Highland parametrization and the introduction of a new alternative algorithm derived from Molière's multiple scattering law (chap. 3).

The introduction of a new random number transformation method leads to a crucial reduction of the required computation time for the Highland approximation (see chap. 4.3). An easy and fast way to compute multiple scatterings following Molière's theory has been developed, showing a better agreement with measurement data than the current algorithm. Especially the occurence of large-angle scatters is better described by the new algorithm 4.1 .

It is strongly advised to take into account multiple scattering in future muon simulations involving PROPOSAL for it could be shown in chap. 4.2 that the resulting displacements from the shower axis are distinctly larger than expected by [6, 14] . The Molière-based algorithm should be used in order to increase the simulation's accuracy, but provided high requirements are imposed on the computation time, the new Highland code grants comparatively big timesavings (about $\sim$ 20 times faster than the Molière code for scatterings in ice, see chap. 4.3).

5.2 Prospect

The developed methods described here are now ready to be used when working with PROPOSAL. Future work on the multiple scattering algorithms could concentrate on the overestimation of the probability of large scattering angles. A reasonable parametrization would need to be found, if a cut-off angle was to be introduced (cf. chap. 4.1).

A considerably higher calculation precision could be achieved by employing higher terms of Molière's sequence (2.2.21) in the series expansion of Molière's probability density (2.2.20) as shown by [35]. Therefore, the integrals (2.2.21) could be numerically calculated in order to tabulate sampling points for interpolation methods. Maybe a correspondingly modified random angle generator could even lead to a reduced computation time.

Furthermore, modifications to Molière's theory could be applied (e.g. Fano (1954) [36]). It might be worth trying to introduce a finite nuclear size, a more accurate screened potential, or try to give up the assumption of incoherent scatterings (cf. chap. 2.2 and 2.1), but all these modifications are likely to destroy the simplicity of Molière's theory and thus might vitally compromise the computations speed.

A sophisticated and extensive verifying and benchmarking of the implemented algorithms is compromised by the lack of extensive modern research in the field of muon multiple scattering. Most of the theoretical work has been done more than 60 years ago. There is simply no data to be found covering several energy intervals or a variety of scattering media in an up-to-date measurement accuracy. Dedicated experiments to fill that gap would be very helpful and valuable, and certainly much appreciated.

6 Acknowledgment

- I'd like to express my gratitude to Tomasz Fuchs and Jan-Hendrik Köhne for their guidance, advice and support. They have always been very competent, helpful, kind and active in case I had physical, mathematical and programming questions and patient while introducing me to IceCube and PROPOSAL. I'd also like to thank them for the final build-in of my code.
- As well, I thank Prof. Dr. Dr. Wolfgang Rhode for his supervision and inspiring impulses the thesis benefited from.
- Thanks go to Tomasz Fuchs, Ann Kathrin Torheiden and Mark Aartsen for looking over my writings.
- I thank Prof. Dr. Bernhard Spaan for his efforts as second corrector.
- Gratefully, I appreciate the help of Robin Ponte and my parents, who were making for a fast and uncomplicated transmission and submission of this thesis that was finished in Stockholm.
- Last but not least, I wish to thank the whole workgroup of EVb for the pleasant and supportive working atmosphere.

Figures

All the plots and pictures in this bachelor thesis without explicit reference have been created by the author. Used software tools were the programs ROOT 5.34, GIMP 2.8.4 and LibreOffice Draw 4.0.2.2 .

List of Figures

List of Tables

References

[1] J. Beatty. The Pierre Auger project: An observatory for the highest energy cosmic rays. *Nuclear Instruments and Methods in Physics Research A*, 16:1022, 2001.

[2] C. Bigongiari. The MAGIC telescope. In *International Europhysics Conference on High Energy Physics, HEP2005*, 2005.

[3] F. Halzen. Neutrinos Associated with Cosmic Rays. *Journal of Physics: Conference Series*, 337:012050, 2012.

[4] V. Cirkel-Bartelt. History of astroparticle physics and its components. *Living Reviews in Relativity*, 11(2), 2008.

[5] C. Spiering. High Energy Neutrino Astronomy: Status and Perspectives. In *American Institute of Physics Conference Series*, volume 1085 of *American Institute of Physics Conference Series*, 2008.

[6] J.-H. Köhne, K. Frantzen, M. Schmitz, T. Fuchs, W. Rhode, et al. PROPOSAL: A tool for propagation of charged leptons. *Computer Physics Communications*, 184:2070, 2013.

[7] M. Ageron et al. ANTARES: The first undersea neutrino telescope. *Nuclear Instruments and Methods in Physics Research A*, 656:11, 2011.

[8] The Km3NeT consortium. The KM3NeT Project. *Journal of Physics: Conference Series*, 375:052036, 2012.

[9] E. Andres et al. The AMANDA neutrino telescope: principle of operation and first results. *Astroparticle Physics*, 13:1, 2000.

[10] A. Achterberg et al. First year performance of the IceCube neutrino telescope. *Astroparticle Physics*, 26:155, 2006.

[11] R. Abbasi et al. IceTop: The surface component of IceCube. *Nuclear Instruments and Methods in Physics Research A*, 700:188, 2013.

[12] R. Abbasi et al. The design and performance of IceCube DeepCore. *Astroparticle Physics*, 35:615, 2012.

[13] Williams, D. The Precision IceCube Next Generation Upgrade. *arXiv:1310.1287v1*, October 2013.

[14] D. Chirkin and W. Rhode. Propagating leptons through matter with Muon Monte Carlo (MMC). *arXiv:hep-ph/0407075v2*, July 2004.

[15] "scattering (physics)". *Encyclopædia Britannica Online*. Encyclopædia Britannica Inc., http://global.britannica.com/EBchecked/topic/526813/scattering, October 2013.

[16] G. Molière. Theorie der Streuung schneller geladener Teilchen II. Mehrfach- und Vielfachstreuung. *Zeitschrift Naturforschung Teil A*, 3:78, 1948.

[17] G. Wentzel. Zur Theorie der Streuung von β-Strahlen. *Annalen der Physik*, 69:335, 1922.

[18] S. Goudsmit and J. Saunderson. Multiple Scattering of Electrons. *Physical Review*, 57:24, 1940.

[19] H. Lewis. Multiple Scattering in an Infinite Medium. *Physical Review*, 78:526, 1950.

[20] G. Molière. Theorie der Streuung schneller geladener Teilchen I. Einzelstreuung am abgeschirmten Coulomb-Feld. *Zeitschrift Naturforschung Teil A*, 2:133, 1947.

[21] A. Butkevich, R. Kokoulin, et al. Comments on multiple scattering of high-energy muons in thick layers. *Nuclear Instruments and Methods in Physics Research Section A*, 488:282, 2002.

[22] G. Lynch and O. Dahl. Approximations to multiple Coulomb scattering. *Nuclear Instruments and Methods in Physics Research Section B*, 58:6, 1991.

[23] H. Bethe. Molière's theory of multiple scattering. *Physical Review*, 89:1256, 1953.

[24] B. Gottschalk et al. Multiple Coulomb scattering of 160 MeV protons. *Nuclear Instruments and Methods in Physics Research B*, 74:467, 1993.

[25] W. Simon. Verification of molière's theory of multiple scattering for heavy ions. *Physical Review*, 136:B410, 1964.

[26] W. Scott. The Theory of Small-Angle Multiple Scattering of Fast Charged Particles. *Reviews of Modern Physics*, 35:231, 1963.

[27] B. Rossi and K. Greisen. Cosmic-Ray Theory. *Reviews of Modern Physics*, 13:240, 1941.

[28] V. Highland. Some practical remarks on multiple scattering. *Nuclear Instruments and Methods*, 129:497, 1975.

[29] D. Attwood et al. The scattering of muons in low-Z materials. *Nuclear Instruments and Methods in Physics Research Section B*, 251:41, 2006.

[30] B. Schneider. Algorithm AS 121: Trigamma Function. *Journal of the Royal Statistical Society Series C*, 27:97, 1978.

[31] K. Nakamura et al. Review of Particle Physics. *Journal of Physics G*, 37:075021, 2010.

[32] Y. Tsai. Pair production and bremsstrahlung of charged leptons. *Reviews of Modern Physics*, 46:815, 1974.

[33] H. Davies, H. Bethe, and L. Maximon. Theory of Bremsstrahlung and Pair Production. II. Integral Cross Section for Pair Production. *Physical Review*, 93:788, 1954.

[34] S. Akimenko, V. Belousov, et al. Multiple Coulomb scattering of 7.3 and 11.7 GeV/c muons on a Cu target. *Nuclear Instruments and Methods in Physics Research Section A*, 243:518, 1986.

[35] P. Andreo, J. Medin, and A. Bielajew. Constraints of the multiple-scattering theory of Molière in Monte Carlo simulations of the transport of charged particles. *Medical Physics*, 20:1315, 1993.

[36] U. Fano. Inelastic Collisions and the Molière Theory of Multiple Scattering. *Physical Review*, 93:117, 1954.